WORLD RESOURCES INSTITUTE

TECHNICAL NOTE

Estimating future local climate hazard probabilities

Theodore Wong and Paul Switzer

CONTENTS

Abstract....1
Background....1
Data....3
Climate model selection and calibration 5
Estimates of climate hazard frequencies and their uncertainty....6
Examples....8
Applications....18
Limitations....19
Endnotes....20
Abbreviations....20
References....20
Acknowledgments....22
About the authors....22
About WRI....22

Technical notes document the research or analytical methodology underpinning a publication, interactive application, or tool.

Suggested Citation: Wong, T., and P Switzer. 2023. "Estimating future local climate hazard probabilities." Technical Note. Washington, DC: World Resources Institute. Available online at: doi.org/10.46830/writn.22.00074.

ABSTRACT

Decision-makers in government, the private sector, and civil society can better plan for climate change if their decisions are informed by predictions of future climate conditions and meteorological events as well as information about prediction uncertainty. This technical note describes a probabilistic method for predicting geographically localized future climate hazard events using output from downscaled climate models. The method provides probabilistic estimates of how often a given location will experience a prescribed climate hazard event or indicator during a prescribed future planning period, as defined by a user. Insights from this process can support climate adaptation and disaster risk reduction planning in agriculture, infrastructure, public health, and other domains.

BACKGROUND

Decision-making that involves land, built assets, or human populations must confront how the local climate will change. Long standing societal systems such as cities and agriculture have adapted to long-existing climate regimes. Climate change has already begun disrupting these systems, and the increasing frequency of disruptive meteorological conditions and events has already attracted the concern of researchers and practitioners in food security (Thornton et al. 2014), transportation infrastructure (Nasr et al. 2019; Wang et al. 2019), energy infrastructure (Burillo et al. 2017), emergency management (Arnell 2022), worker safety (Moda et al. 2019), public health (Ngonghala et al. 2021; Rocklöv and Tozan 2019), and other domains of human activity.

Global climate models provide readily available information on climate futures, but this information can be difficult for decision-makers to apply to their particular needs. For example, consider a roadway engineer who wants to know whether current local pavement design standards will be adequate under the future precipitation regime. Specifically, it might be useful to know how often

to expect "extreme" precipitation events for the planning period 2050–90, where an extreme precipitation event is defined as an accumulation greater than a specified threshold, perhaps over a four-day period. Climate models do not output annual frequencies of events such as four-day threshold exceedances but rather as hourly, daily, or monthly instances of raw meteorological variables in a number of simulations. To convert these simulation outputs into estimates of frequencies of complicated climate hazard events is nontrivial.

The hypothetical roadway engineer will also need information regarding the uncertainty of the prediction. Some decisions—for example, whether to invest in redundant systems or whether to purchase insurance—depend not only on hazard predictions but also on prediction uncertainty.

The goal of this paper is to provide estimates of the frequencies of localized climate hazard events for a specified future period, together with a representation of the uncertainty of such estimates, based on information provided by available climate models. Climate models are built on numerous assumptions, and their outputs include an enormous amount of uncertainty. Our method does not remove this uncertainty; rather, it expresses it in terms of probabilities of climate events.

The climate hazard events that are considered here are those whose occurrences can be seen or derived from the four parallel daily time series of minimum temperature, maximum temperature, daily precipitation, and daily average relative humidity. In addition, hazard events may also be defined in terms of a daily time series calculated from two or more of these four aforementioned time series, such as a thermal comfort index that combines daily temperature and humidity.

These are some examples of hazard definitions:

- Yearlong precipitation exceeding 1,800 millimeters
- Runs of five or more consecutive days with maximum wet-bulb globe temperature exceeding 35°C
- Sixty or more consecutive days with zero precipitation
- Accumulation of 3,000 growing degree-days between a crop's planting date and the first autumn frost

Estimates of the frequency of future hazard events can be obtained from the daily time series output of any of the numerous climate models. There will be inevitable disagreement among these climate models, and there are potential biases introduced when coarse-scale global models are downscaled to estimate higher-resolution climate phenomena. We deal with model disagreement by focusing on those downscaled models that most closely agree with matching observational data during the historical calibration period 1980–2014 (see "Estimates of climate hazard frequencies and their uncertainty"). Model selection will depend on both the geographic location and the specific weather variable(s) involved in the hazard specification. Further, the weather time series of the selected downscaled climate models are calibrated so that the calibrated model data match the statistics of the observational data (see "Climate model selection and calibration").

However, all climate models carry inherent uncertainty in their future predictions, which is characterized probabilistically. Basically, a climate model's future hazard event count is treated as a realization of a random variable, and Bayes methodology is then used as a framework for generating a distribution of possible future hazard event counts as an expression of the prediction uncertainty. (This probabilistic framework is more fully described in "Estimates of climate hazard frequencies and their uncertainty.")

Project background

The method was developed to produce hazard information for climate adaptation as part of the Data Portal for Cities project (GCoM 2023), which is a partnership between World Resources Institute (WRI) and the Global Covenant of Mayors for Climate and Energy (GCoM). GCoM member cities are expected to report future climate hazard probabilities under GCoM's Common Reporting Framework (GCoM 2018). This method provides a method for calculating those probabilities.

Existing data resources provide climate hazard forecasts, but without some useful detail that our method can provide. Some, such as the Climate Change Knowledge Portal (World Bank n.d.) and the Intergovernmental Panel on Climate Change Working Group I Atlas (Iturbide et al. 2021), provide simple meteorological variable predictions. The ThinkHazard! tool provides ordinal (i.e., *high*, *medium*, *low*, and *very low*) risk assessments based on probabilities of predefined indicators and thresholds.[1] It does not allow users to choose indicators or critical thresholds. Our method differs from these approaches in its ability to allow data tools to report exceedance probabilities based on indicators and thresholds provided by, and presumably directly relevant to, users.

This method has been piloted using hazard definitions identified in collaboration with GCoM, four GCoM cities (Hobart, Australia; Makati, Philippines; Tópaga, Colombia; and Vitacura, Chile), and stakeholders in an integrated climate assessment process in Campinas, Brazil. It is also being piloted in data dashboards for the UrbanShift and Cities4Forests platforms,

for the prototype AgriAdapt agricultural climate risk assessment tool funded by the Walmart Foundation, and a project supported by Bloomberg Philanthropies to describe city climate hazards under 1.5°C and 2.0°C global warming scenarios.

DATA

Data sources

This method requires two types of data, both time series of daily meteorological variables, downscaled to a level of spatial resolution suitable for the eventual application. One set of time series, used for climate model calibration, are historical observations for the years 1980–2014. For this, we use the ERA5 reanalysis data set (ECMWF 2022), a satellite data product of the European Centre for Medium-Range Weather Forecasts with a spatial resolution of 31 kilometers (km). The other data set is an ensemble of downscaled daily time series outputs from global climate models (GCMs). These time series include the historical years covered by the observation time series as well as the specified future years of interest. We have used the National Aeronautics and Space Administration (NASA) NEX-GDDP-CMIP6 product (NASA 2023), which includes outputs from 34 Coupled Model Intercomparison Project Phase 6 (CMIP6) models at approximately 25 km spatial resolution. CMIP6 is a project that coordinates among research institutions to standardize model outputs to allow for intercomparison (Eyring 2016). Of the 34 models included in NEX-GDDP-CMIP6, 30 include all variables of interest for all years of interest. These models are listed in Table 1.

Table 1 also lists a model family for each included model. Kuma et al. (2023) find that many of the climate models included in model intercomparison projects share algorithms and code. This is because research institutions commonly share modular code components among each other, and researchers commonly reuse code as they develop newer generations of models. Combining or comparing results from different models will likely underestimate variation if one fails to account for the underlying similarity among models that share a family. As we describe below, our strategy here is to ensure that we always report results

Table 1 | **Climate models included in NEX-GDDP-CMIP6**

MODEL	MODEL FAMILY[a]	INSTITUTION[b]
ACCESS-CM2	HadAM	Commonwealth Scientific and Industrial Research Organisation (CSIRO); Australian Research Council Centre of Excellence for Climate System Science
ACCESS-ESM1-5	HadAM	CSIRO
BCC-CSM2-MR	CCM	Beijing Climate Center
CanESM5	CanAM	Canadian Centre for Climate Modelling and Analysis
CMCC-CM2-SR5	CCM	Fondazione Centro Euro-Mediterraneo sui Cambiamenti Climatici
CMCC-ESM2	CCM	
CNRM-CM6-1	ECMWF	Centre National de Recherches Meteorologiques; Centre Européen de Recherche et de Formation Avancée en Calcul Scientifique
CNRM-ESM2-1	ECMWF	
EC-Earth3	ECMWF	EC-Earth Consortium (Agencia Estatal de Meteorología, Spain; Barcelona Supercomputing Center, Spain; Consiglio Nazionale delle Ricerche–Istituto di Scienze dell'Atmosfera e del Clima, Italy; Danish Meteorological Institute, Denmark; Ente per le Nuove Technologie l'Energia e l'Ambiente, Italy; Finnish Meteorological Institute, Finland; Geomar, Germany; Irish Centre for High-End Computing, Ireland; International Centre for Theoretical Physics, Italy; Instituto Dom Luiz, Portugal; Institute for Marine and Atmospheric research Utrecht, Netherlands; Instituto Português do Mar e da Atmosfera, Portugal; Karlsruhe Institute of Technology, Germany; Royal Netherlands Meteorological Institute, Netherlands; Lund University, Sweden; Met Eireann, Ireland; Netherlands eScience Center, Netherlands; Norwegian University of Science and Technology, Norway; Oxford University, UK; SURFsara, Netherlands; Swedish Meteorological and Hydrological Institute, Sweden; Stockholm University, Sweden; Unite ASTR, Belgium; University College Dublin, Ireland; University of Bergen, Norway; University of Copenhagen, Denmark; University of Helsinki, Finland; University of Santiago de Compostela, Spain; Uppsala University, Sweden; Utrecht University, Netherlands; Vrije Universiteit Amsterdam, Netherlands; Wageningen University, Netherlands)
EC-Earth3-Veg-LR	ECMWF	
FGOALS-g3	CCM	Chinese Academy of Sciences

Table 1 | **Climate models included in NEX-GDDP-CMIP6 (continued)**

MODEL	MODEL FAMILY[a]	INSTITUTION[b]
GFDL-CM4	GFDL	National Oceanic and Atmospheric Administration (United States), Geophysical Fluid Dynamics Laboratory
GFDL-CM4_gr2	GFDL	
GFDL-ESM4	GFDL	
HadGEM3-GC31-LL	HadAM	Met Office Hadley Centre; Natural Environment Research Council (United Kingdom)
HadGEM3-GC31-MM	HadAM	Met Office Hadley Centre; Natural Environment Research Council (United Kingdom); National Institute of Meteorological Sciences/Korea Meteorological Administration
INM-CM4-8	INM	Institute for Numerical Mathematics, Russian Academy of Science
INM-CM5-0	INM	
IPSL-CM6A-LR	IPSL	Institut Pierre Simon Laplace
KACE-1-0-G	HadAM	National Institute of Meteorological Sciences/Korea Meteorological Administration; National Institute of Water and Atmospheric Research (New Zealand)
KIOST-ESM	GFDL	Korea Institute of Ocean Science and Technology
MIROC6	MIROC	Japan Agency for Marine-Earth Science and Technology
MIROC-ES2L	MIROC	
MPI-ESM1-2-HR	ECMWF	HAMMOZ Consortium (ETH Zurich, Switzerland; Max Planck Institut für Meteorologie, Germany; Forschungszentrum Jülich, Germany; University of Oxford, United Kingdom; Finnish Meteorological Institute, Finland; Leibniz Institute for Tropospheric Research, Germany; Center for Climate Systems Modeling, ETH Zurich, Switzerland)
MPI-ESM1-2-LR	ECMWF	
MRI-ESM2-0	UCLA GCM	Meteorological Research Institute (Japan)
NorESM2-LM	CCM	NorESM Climate Modeling Consortium (Center for International Climate and Environmental Research; Norwegian Meteorological Institute; Nansen Environmental and Remote Sensing Center; Norwegian Institute for Air Research; University of Bergen; University of Oslo; and Uni Research)
NorESM2-MM	CCM	
TaiESM1	CCM	Research Center for Environmental Changes, Academia Sinica
UKESM1-0-LL	HadAM	Met Office Hadley Centre; Natural Environment Research Council (United Kingdom); National Institute of Meteorological Sciences/Korea Meteorological Administration

Note: We acknowledge the World Climate Research Programme, which, through its Working Group on Coupled Modelling, coordinated and promoted CMIP6. We thank the climate modeling groups for producing and making available their model output, the Earth System Grid Federation (ESGF) for archiving the data and providing access, and the multiple funding agencies who support CMIP6 and ESGF.

Sources: a. Kuma et al. 2023; b. NASA 2023.

from models from different families. (See Sanderson et al. [2017] for an alternative approach to making use of information from model ensembles.)

NEX-GDDP-CMIP6 provides several greenhouse gas emission scenarios based on the Shared Socioeconomic Pathways (SSPs; Riahi et al. 2017) We used SSP5-8.5, which incorporates the high emissions scenario that most closely reflects both historical emissions and plausible scenarios of future emissions (Schwalm 2020). In the CMIP6 models, the emission pathways are used only for years beginning with 2015. For years 2014 and prior, atmospheric composition is driven by historical natural and human-driven processes. Our selected historical year range ends with 2014 to allow us to separate our consideration of historical and emission-driven climates.

Occurrences of specified hazard events are determined from the daily time series of the relevant weather variables, such as the maximum daily near-surface air temperature, minimum daily temperature, and daily precipitation.

CLIMATE MODEL SELECTION AND CALIBRATION

Climate model selection

We select those climate models that perform best for a particular weather variable in a particular geographic location. Model output time series are compared with the corresponding observed time series over the historical period 1980–2014. We divide the 35-year historical period into 140 quarterly seasons and find each season's mean value for the weather variable of interest. We compute the root-mean-square error (RMSE) difference between the 140 quarterly mean values for the model output and the corresponding 140 historical average values. We do this for each of 30 NEX-GDDP-CMIP6 models and rank the models according to their RMSE when compared with observations for the historical period. The goal is to select downscaled models that best match the relevant weather variable seasonal climatology of the observations at the specified location, not to match day-by-day observations.

To present concise model-based estimates of the frequency of future hazard events and reduce the computational burden of subsequent calculation, we select the three climate models with the smallest RMSE when compared with corresponding observations for the historical period 1980–2014. We further constrain the selection of climate models to ensure that they are from three different model families. Selection is implemented as follows:

1. For each model family, rank the member models by RMSE.
2. Rank the families by the smallest RMSE of their members.
3. Select as the best models the best members of the three best families.

When selecting the best models, the decision will depend both on the specified geographic location and the particular weather variable relevant to the specified hazard event definition. For hazards that combine more than one weather variable, the user must decide which model(s) to use for each of the component variables, and whether and how to combine them. Further research is needed to understand the benefits and drawbacks of using one high-performing model for all the weather variables that compose the indicator or for various methods of combining different high-performing models for each weather variable.

Climate model calibration

We then calibrate the best models to better align with the historical data; that is, we shift the climate model output data to more closely align with the distribution of the historical data. To do so, for each of the selected climate models, the relevant weather variable data are recalibrated so that the marginal frequency distribution of the pooled daily values of calibrated model data approximately matches the marginal frequency distribution of the corresponding pooled observed data for the historical period 1980–2014. The marginal distribution of time series data is the frequency distribution of the daily weather variable measurements considered as a pooled sample of numbers.

We align the model frequency distribution with the historical data by shifting the percentiles of the model distribution. For example, if the 20th model percentile corresponds to the 30th percentile of the observations, then the 30th percentile of the *calibrated* model data will correspond to the 20th percentile of the uncalibrated model data. The calibration is achieved using percentile-percentile (P-P) plots. (See Holmgren [1995] for a discussion of P-P plots.) Specifically, a P-P plot shows the fraction of the observed daily values (horizontal axis) that are less than or equal to the p percentile of the model data (vertical axis), for values of p between zero and 100 percent. P-P calibration is described algorithmically below.

The flexibility of percentile calibration allows for model data to shift both higher and lower in different parts of the distribution. Although common methods of calibrating model data to observations typically use parametric linear regressions, we chose to adapt nonparametric P-P plots for calibration because of their flexibility over the whole range of weather data. Percentile calibration also avoids having to make arbitrary adjustments to parametric methods when they result in impossible values (e.g., negative counts).

The following is an algorithmic description of the P-P calibration plot construction. The horizontal and vertical axes of a P-P plot run from 0 to 1, respectively, representing the cumulative fractions of the observed and modeled historical weather variable data. Ignoring leap years, there are some daily values of the weather variable during the 35-year calibration period.

1. Pool all the daily data, combining the observed and model data, and sort the pooled data from small to large.
2. Let $O(j)$ be the position in the combined sorted data of the smallest value in the sorted unpooled *observed* data.

3. The P-P calibration plot is a nondecreasing plot with N plotted points whose coordinates are

$$\left(\frac{j}{N+1}, \frac{O(j)-j+1}{N+1}\right) \text{ for } j = 1..N$$

Effective P-P model calibration requires substantial overlap of the historical frequency distributions of the selected model weather data and corresponding observations at the specified location. Models were selected based on how well they matched the historical period weather data; nevertheless, a selected model may be a bad match to marginal distribution of the observations. Therefore, model predictions for future time periods should not be attempted with output from that model. P-P calibration will not correct gross model inadequacy. As a suggested arbitrary rule of thumb, the smallest of the modeled daily weather values for the historical calibration period should not exceed the 10th percentile of the observed values, and the largest of the modeled values should not fall below the 90th percentile of the observed values, with at least 80 percent overlap between observations and selected-model data. In our examples, insufficient distributional overlap was not encountered.

We derive four separate P-P calibration plots that are specific to data from each season, defined as March–May, June–August, September–November, and December–February, and each quarter includes 3,285 daily values of observed or model data, for each weather variable, in the historical period. P-P plots are further specific to the selected climate model, geographic location, and the relevant weather variable. The P-P calibration plots derived from the historical data are then used to recalibrate the future period daily weather variable time series generated by the selected climate models. The four seasonal P-P calibration plots are then used to shift the marginal distribution of future model-generated daily weather data, separately for each season, for the specified future hazard prediction period. The method of using the P-P plots to calibrate future model data is described algorithmically below.

Application of the P-P plot to calibration of future model weather data

Future daily weather time series, derived from a selected climate model for a specified future period, are recalibrated using the previously described P-P calibration plots that were estimated from past historical data. Recalibration is done separately for the pooled model data from each of the four seasons, using the season-specific P-P plot. The number of season-specific daily values is denoted by N_{fut}; for example, a 20-year future period has approximately N_{fut} = 1825 = 20 × 365 ÷ 4 daily values from each of the four seasons.

First, the daily data are put in size order from small to large. Calibration consists of replacing the j'-th smallest value by the j' smallest value, where j' is calculated using the associated P-P calibration specific to the season and the selected climate model as follows:

1. Set $X(j) = \frac{j}{N_{fut}+1}$ on the horizontal axis of the P-P plot and determine the corresponding vertical coordinate $Y(j)$ from the P-P plot. (N_{fut} = 1825.)
2. Set $j' = Y(j) \cdot (N_{fut} + 1)$ (i.e., replace the j-th smallest future model value by the j'-th smallest future value).
3. Repeat this model data shifting for each $j = 1..N_{fut}$ (Note: Some of the very smallest or very largest of the calibrated data values may repeat.)

Finally, put combined shifted model values back into their original time order to obtain the calibrated model daily time series for the specified future period. The calibrated model future time series is then scanned to obtain a count of the number of predicted events. This future data calibration exercise is repeated for each of the three selected climate models.

ESTIMATES OF CLIMATE HAZARD FREQUENCIES AND THEIR UNCERTAINTY

The goal is to predict the number of occurrences of a specified climate hazard event during a specified future period at a specified geographic location. In general, to obtain the future hazard frequency estimate for a selected climate model, we calibrate the relevant future model weather data and then scan the resulting calibrated daily time series to obtain the model-estimated count of the number of hazard events during the specified future period. This event count derived from the future calibrated model time series is denoted by C. The statistical uncertainty associated with this predicted future event count derives from the probabilistic framework described below.

The uncertainty assessment of future model-based event counts is based on probabilistic assumptions. Here we assume that hazard events occur over time according to a nonhomogeneous Poisson stochastic process that is governed by an unknown rate parameter. This rate parameter could vary year to year over the duration of the specified future prediction period (thus making it nonhomogeneous) to reflect ongoing climate evolution. The

Poisson rate parameter could also vary seasonally. The time-integrated value of this uncertain rate parameter is denoted by *r*. The number of event occurrences over the specified future period is then a Poisson-distributed random variable with mean *r*. (The Poisson process framework does restrict the type of hazard events that can be considered. Specifically, it excludes events that are expected to occur clustered in time. For such cases, counts of individual events could be replaced by counts of event clusters, suitably defined.)

Cast in a Bayes framework, we use the Jeffreys invariant prior distribution for the unknown Poisson distribution parameter, *r*. Then, conditioning on the future event count, *C*, obtained from the calibrated model data, will yield a gamma posterior distribution for the Poisson distribution parameter, *r*. This posterior gamma distribution for *r* has mean $C + {}^1/_2$.

To represent the uncertainty in the future event count, based on the selected climate model, we use the resulting Bayes predictive frequency distribution. This distribution is a form of the gamma-Poisson distribution where the probability of seeing *x* events during the future period is

$$p(x) = \frac{({}^1/_2)^{x+C+{}^1/_2} \cdot \mathrm{G}(x + C + {}^1/_2)}{\mathrm{G}(C + {}^1/_2) \cdot \mathrm{G}(x + 1)} \text{ for } x = 0, 1, 2 \ldots$$

where G denotes the gamma function. This distribution is left skewed with mean $C + {}^1/_2$, and standard deviation is $\sqrt{2C + 1}$. This frequency distribution of predicted event counts can be graphically represented by its histogram (see "Illustration: Nairobi drought"). This distribution of future hazard event counts can also be used to obtain probabilities of specified outcomes of interest, such as the probability of experiencing at least *x* hazard events during the specified future period.

Hazard event counts for the specified future prediction period can also be expressed as average annual counts by dividing by *N*, the length in years of the specified future period.

The event count prediction exercise described above is repeated for each of the three selected climate models chosen for the specified hazard definition at the specified location. Hazard event count prediction distributions that are derived from different climate models will differ more or less from one another; we report results for the three selected models to illustrate the degree to which the climate models might differ in their predictions. There is no simple statistical basis for combining results from different climate models. (See "Limitations," where we further discuss the issue of combining or not combining predictions from different climate models).

These future hazard event count uncertainties are conditional on the model calibration P-P plots derived from the historical calibration period. These calibration plots shift daily model weather data so that they match the 40-year marginal frequency distribution of the historical daily data. If we had access in our downscaled data set to multiple, independent runs of each model, then the hazard event prediction exercise, including calibration, could be repeated separately for each ensemble member, and the predicted future hazard event counts would be pooled across all ensemble members. The pooled event counts would then also include variation induced by variability among the calibration plots. However, given the 40-year length of the historical calibration period, we would not expect large differences among calibration plots for different ensemble members from the same model.

Zero-one annual count data

If hazard events are defined as occurring or not occurring during a calendar year, then a more appropriate probabilistic formulation of event count uncertainty treats each year as a Bernoulli trial with event occurrence probabilities *p* and (1 - *p*), respectively. For example, a hazard event year might be one having at least 10 days with a maximum temperature of 40°C or higher, as in the Kolkata illustration described in the "Examples" section. The goal is to provide a prediction for the number of future-period years that experience the hazard event, together with a range of uncertainty based on probability modeling of event occurrences. For the Kolkata example, hazard event occurrences are derived from the maximum temperature daily time series; climate model selection and calibration to historical maximum temperature data are the same as previously described.

For the specified future period, such as the 21-year period 2050–70, we obtain the model daily time series of the relevant weather variable, which is then recalibrated separately for each of the selected downscaled climate models. We use the recalibrated daily time series to obtain a count, *C*, of the number of years that meet the specified hazard event definition.

If the annual event occurrence probability *p* is assumed not to change during the *N*-year future prediction period, then the total number of years with event occurrences would be a binomial random variable with parameters *N* and *p*. The assumption is also that the occurrence of the event in one year does not affect the event occurrence probability in another year. These independence assumptions are less restrictive than the requirements described earlier for Poisson modeling of event occurrences.

With this probabilistic structure for future event occurrences, our Bayes formulation treats the binomial event-rate parameter, p , as itself random with a Jeffreys invariant prior distribution. Then the posterior distribution of the future period p, conditional on the model event count, C, is a beta distribution with parameters $C + 1/2$, $\beta = N - C + 1/2$.

The resulting uncertainty distribution of the future period hazard event count, derived from the selected climate model, is represented by the Bayes predictive frequency distribution. This distribution is the beta-binomial distribution where the probability of seeing x hazard years out of N years is

$$\binom{N}{x} \frac{\mathrm{B}(x+\alpha, N-x+\beta)}{\mathrm{B}(\alpha,\beta)} \quad \text{for } x = 0, 1, 2 \ldots$$

The mean of this distribution of hazard event counts is $(C + 1/2) \cdot N/(N+1)$; the standard deviation is

$$\sqrt{\frac{N(C+1/2)(N-C+1/2)(2N+1)}{(N+2)(N+1)^2}}$$

These probabilities for the predicted event counts are represented by a histogram and are repeated for each of the three selected climate models (see "Illustration: Kolkata extreme heat").

Event counts could alternatively be expressed as annual average counts by dividing the counts by N, the length in years of the specified future period. Longer future prediction periods have a smaller coefficient of variation, defined as the prediction standard deviation as a proportion of its mean value.

The Bernoulli annual hazard event occurrence parameter may evolve over the course of the specified future period. If so, the binomial distribution will no longer be strictly correct for describing the total event count over the N-year period. To mitigate the problem, one could divide the future prediction period into a small number of shorter periods—say, decades—and separately record the calibrated model event counts in each decade. The prediction exercise could then be done separately for each decade, yielding separate decadal posterior distributions for the annual rate parameter. The uncertainty associated with the sum of the decadal hazard event counts is represented by the sum of independent beta-binomial distributions.

EXAMPLES

Summary of steps to estimate future climate hazard event occurrence frequencies

1. Specify a geographic location. This method can be applied to only one model pixel at a time. If information for several adjacent pixels is desired, the method would have to be run separately for each pixel.
2. Specify a future period of interest, typically spanning 10–50 years.
3. Specify a hazard event of interest, whose occurrences can be determined from daily time series of minimum temperature, maximum temperature, total precipitation, and average relative humidity.
4. Collect relevant observed daily weather-variable time series for the specified geographic location for the 35-year historical model calibration period 1980–2014.
5. Collect the corresponding daily weather-variable time series for the candidate downscaled climate models.
6. Select the three best candidate models by comparing all candidate models with the observed data for the 35-year historical model calibration period, as described in "Climate model selection and calibration." The following steps are repeated for *each* of the selected climate models.

    i. Compute season-specific P-P calibration plots based on the observations and model data for the historical period.

    ii. For the specified future period of interest, obtain the relevant climate model daily time series for the relevant weather variable. Recalibrate this future period time series using the seasonal P-P calibrations derived from the historical period data.

    iii. For the specified hazard event, count the number of future occurrences in the calibrated daily time series.

    iv. Use the Bayes procedure outlined in "Estimates of climate hazard frequencies and their uncertainty," in conjunction with the calibrated-model future event count, to obtain a posterior frequency distribution for future event counts.

    v. Report the histogram of the future hazard event count, together with appropriate summary statistics. Show these side by side for the three selected models to exhibit model similarities or differences for predicted hazard event counts.

Illustration: Kolkata extreme heat

The first example looks at the frequency of hot weather years in Kolkata, India, during the 21-year period 2050–70. A hot weather year is specified as having 10 or more days with a maximum temperature of 40°C or higher. We chose this event definition for ease of illustration. For example, other heat-related hazard events might be based on a different temperature threshold or a minimum temperature or thermal comfort index. In practice, event definition would be informed by relevant research and consultation with local experts and decision-makers.

Figure 1 presents four annual time series of season-specific daily maximum temperature averages for a location (latitude 22.53° north, longitude 88.36° east) in Kolkata for the years 1980–2014. Seasonal averages are calculated over the three indicated months, and the time series track how the seasonal averages change from year to year. The observed temperature series taken from ERA5 are plotted in yellow. Overall, there are 140 quarters in the historical period for comparing model averages with observed averages to calculate a model's RMSE. The three GCMs with the lowest overall RMSE are plotted in red. The three selected GCM's with the lowest overall RMSE are NorESM2-LM, ACCESS-ESM1-5, and MIROC-ES2L.

Figure 2 shows the four seasonal P-P calibration plots of modeled versus observed daily maximum temperatures at Kolkata for the historical period 1980–2014. The three color-coded plots are for the best-fitting climate models. Future modeled time series of daily maximum temperatures are recalibrated based on these plots (see "Climate model selection and calibration" and "Estimates of climate hazard frequencies and their uncertainty").

Figure 3 plots the daily maximum temperature time series for 2050–70, as modeled by one of the three selected GCMs: NorESM2-LM. Panel A shows the raw output time series, and Panel B shows the corresponding calibrated time series, using the corresponding P-P plots of Figure 2 for calibration. Daily maximum temperatures of 40°C and higher are shaded pink.

For each calendar year in 2050–70 and for each of the selected climate models, we determine whether that year experienced an excessive number of hot days as defined above. The number of such hot years, C, is modeled as the outcome of a binomial distribution with $N = 21$ years and unknown average annual rate parameter p. For the three selected climate models—NorESM2-LM, ACCESS-ESM1-5, and MIROC-ES2L—the Kolkata hot year counts derived from the calibrated climate models for 2050–70 are, respectively, $C = 12$, 18, and 15 years.

Using the probability structure described in "Estimates of climate hazard frequencies and their uncertainty," the posterior probability distribution of the binomial rate parameter is a beta distribution with parameters $\alpha = C + {}^1/_2$, $\beta = N - C + {}^1/_2$. Rather than being uncertainty distributions, these describe the binomial rate parameter for future event counts.

Figure 1 | **Average maximum daily temperature, by seasonal quarter, for a location in Kolkata, India (1980–2014)**

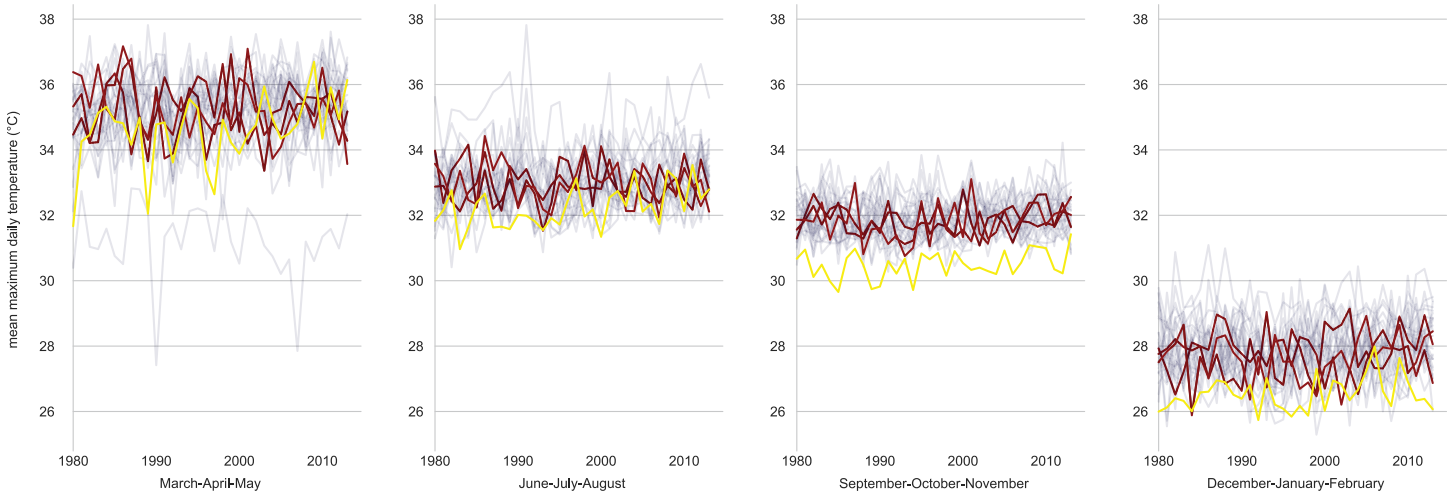

Notes: Observed values from ERA5 are in yellow. Seasonal averages from the three best models are shown in red. Models were selected based on root-mean-square error (RMSE) calculated between modeled and observed quarterly averaged data, across all seasons. These selected models are NorESM2-LM, ACCESS-ESM1-5, and MIROC-ES2L.

Source: WRI authors.

Figure 2 | **P-P plots for each of the selected climate models, based on the marginal distributions of daily maximum temperature in Kolkata (1980–2014)**

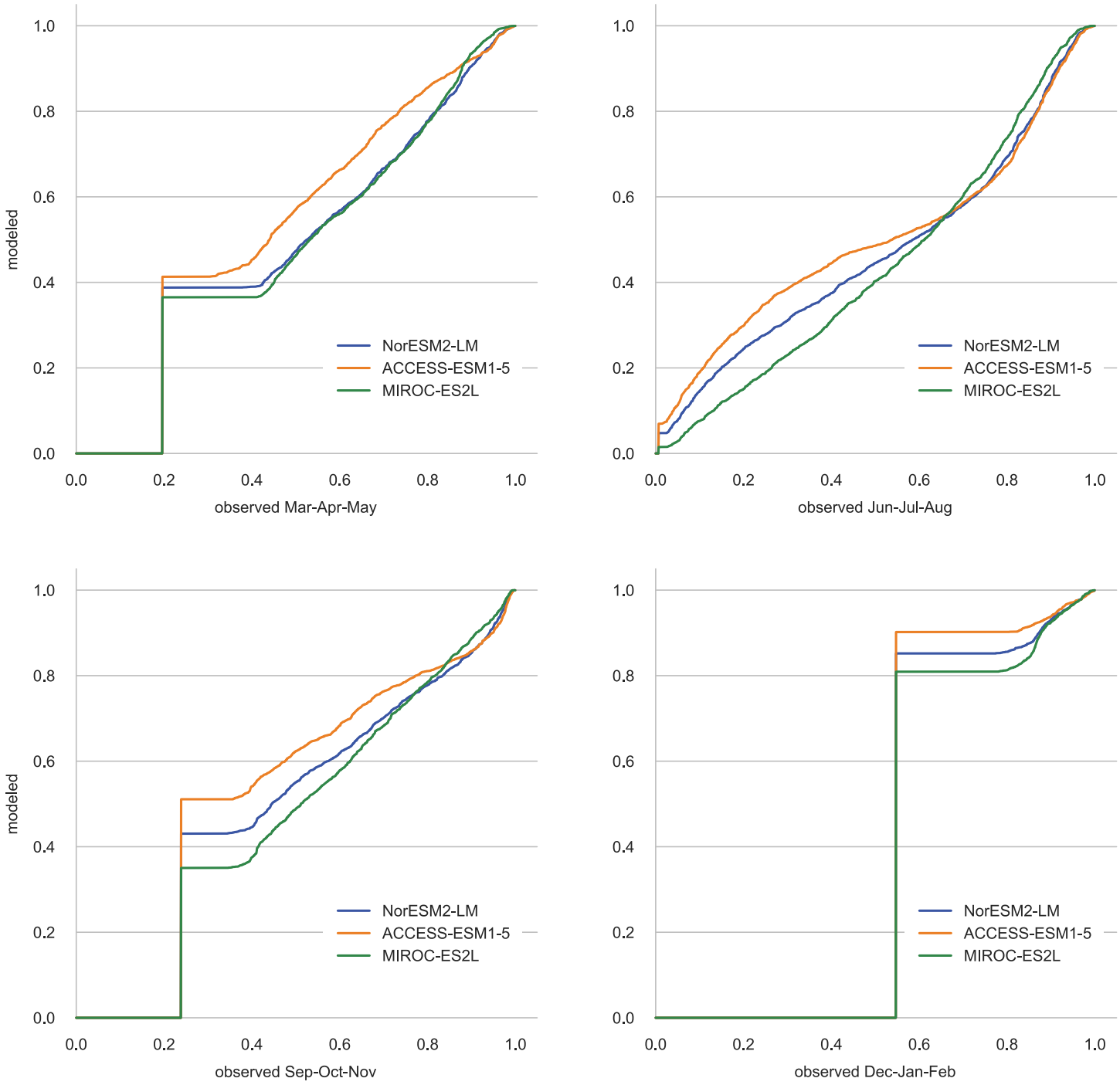

Notes: A percentile-percentile (P-P) plot shows the fraction of the observed daily values (horizontal axis) that are less than or equal to the *p* percentile of the model data (vertical axis). Future period maximum daily temperatures derived from a selected climate model are adjusted based on these plots.

Source: WRI authors.

Figure 3 | **Daily maximum temperatures for Kolkata (2050–2070), derived from the selected model NorESM2-LM**

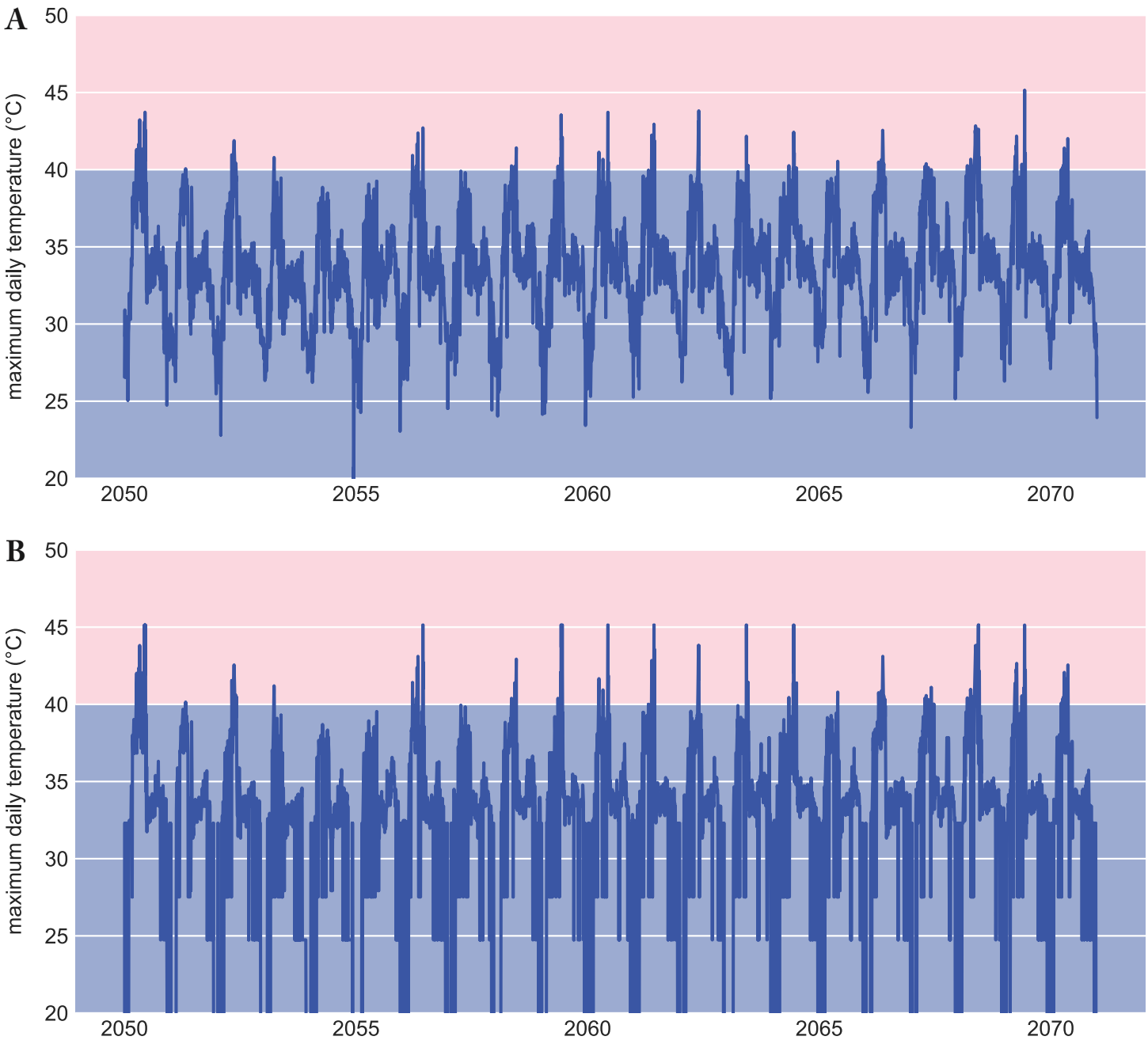

Notes: Temperatures of 40°C and higher are shaded pink. Panel A shows uncalibrated values; Panel B shows values adjusted according to the percentile-percentile calibration plots shown in Figure 2.

Source: WRI authors.

Figure 4 | **Posterior distribution estimates of the frequency of hot years in Kolkata (2050–2070) for each of the three selected climate models**

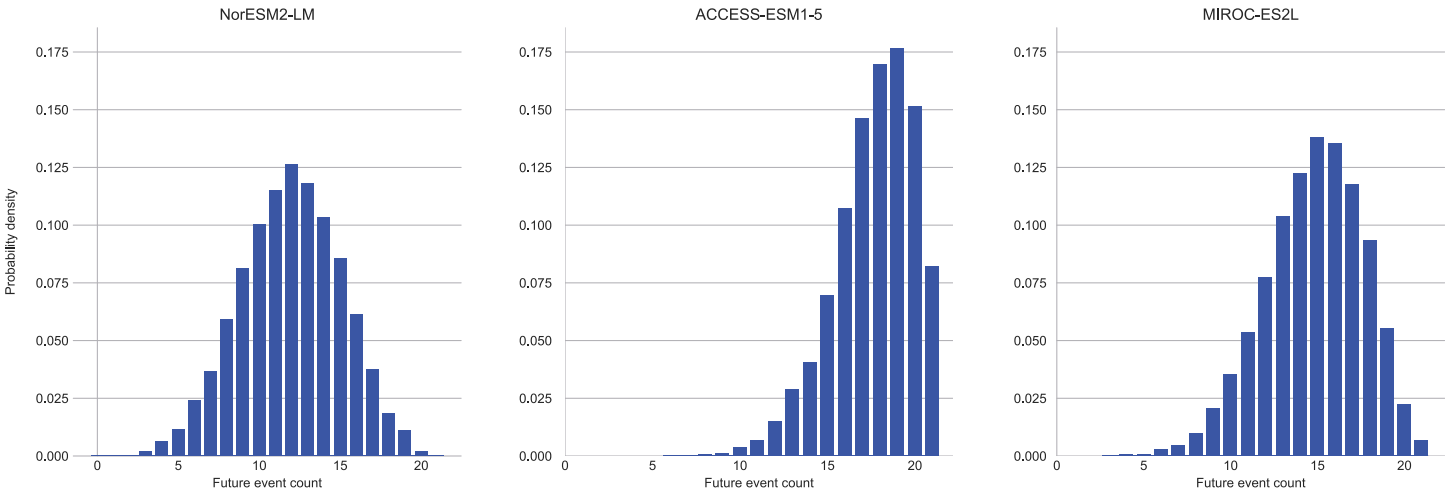

Notes: A hot year event is 10 or more days in a year with maximum temperatures equaling or exceeding 40°C. The frequency-weighted mean number of hot years, calculated from these histograms, are approximately 11.9 years, 17.7 years, and 14.8 years, for the three selected models, respectively. Expressed as percentages of the 21-year period, they are approximately 60 percent, 88 percent, and 74 percent.

Source: WRI authors.

The future event count uncertainty is the beta-binomial distribution described in "Estimates of climate hazard frequencies and their uncertainty," with $N = 21$ and parameters $\alpha = C + {}^1/_2$, $\beta = N - C + {}^1/_2$. Figure 4 shows the histogram of the beta-binomial distribution of predicted counts of future hot year occurrences, together with the corresponding mean predicted counts for the 21-year period 2050–70. We do this separately for each of three selected climate models. The histograms display the uncertainty of these predicted counts, reflecting our probability modeling assumptions. The three recalibrated climate models each produced different future period mean event counts: approximately 11.9 years, 17.7 years, and 14.8 years, respectively. Expressed as percentages of the 21-year period, they are approximately 60 percent, 88 percent, and 74 percent.

Illustration: Nairobi drought

The second example looks at prolonged dry spell events in Nairobi, Kenya. The objective in this example is to estimate the number of dry spells consisting of 15 or more consecutive days with zero precipitation during the period 2050–70. The zero-precipitation and 15-day thresholds were chosen for illustration purposes only; other minimum precipitation thresholds and minimum durations could be specified.

Figure 5 shows the time series of seasonal mean daily precipitation values for a location (latitude -1.28°, longitude 36.82°) in Nairobi, for the historical period 1980–2014. The observed series is plotted in yellow, and the series from the three best models, selected for low RMSE with the observed series, are plotted in red. These three best models are MRI-ESM2-0, IPSL-CM6A-LR, and HadGEM3-GC31-MM.

Figure 6 shows the seasonal P-P calibration plots of modeled versus observed daily precipitation at Nairobi for the historical period 1980–2014. The three color-coded plots are for the three best-fitting climate models. Future modeled precipitation time series are recalibrated based on these plots (see "Climate model selection and calibration" and "Estimates of climate hazard frequencies and their uncertainty").

Figure 7 shows the raw daily precipitation time series as well as the corresponding calibrated time series for 2050–70, output by the downscaled climate model MRI-ESM2-0. This model's historical daily precipitation differs the least from the observed data, using the matching criteria described in "Climate model selection and calibration." The calibrated daily precipitation time series are scanned to obtain counts of the number of hazard event occurrences, which are runs of at least 15 days with zero precipitation. The dry spells are shaded pink in these time series plots. Figure 8 shows the uncalibrated (Panel A) and calibrated (Panel B) daily temperature time series for 2050–70. Panels C and D present close-up views for a single year of daily precipitation data, providing clearer views of the dry spells. The dry spell counts from the calibrated time series are lower than those for the uncalibrated series because the climate models underpredicted daily rainfall amounts for the dry seasons during the historical calibration period.

Figure 5 | **Mean daily precipitation, by seasonal quarter, for a location in Nairobi, Kenya (1980–2014)**

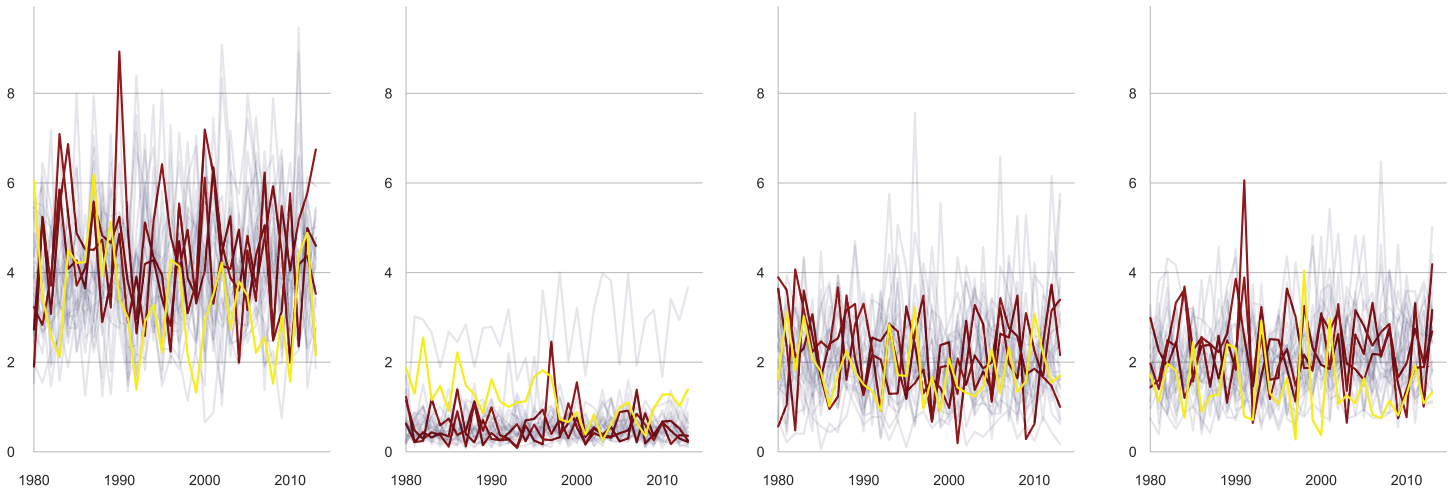

Notes: Observed values from ERA5 are shown in yellow. The values from the three best models, based on root-mean-square error calculated between modeled and observed data, are shown in red.

Source: WRI authors.

Figure 6 | **Quarterly P-P plots for each of the selected climate models based on the marginal distributions of daily total precipitation in Nairobi (1980–2014)**

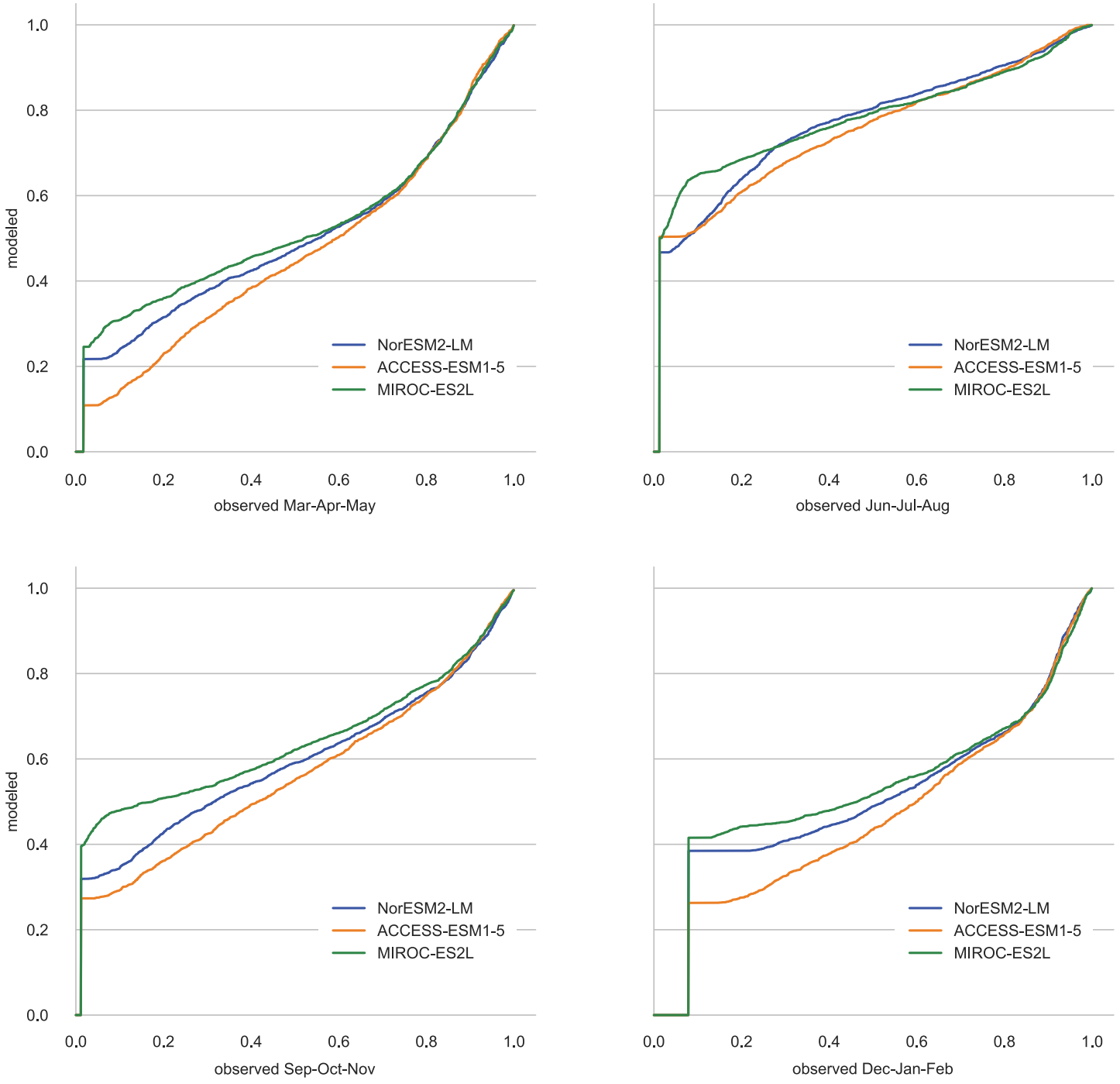

Notes: A percentile-percentile (P-P) plot shows the fraction of the observed daily values (horizontal axis) that are less than or equal to the *p* percentile of the model data (vertical axis). Future period daily precipitation values derived from the selected climate models are adjusted based on these plots.

Source: WRI authors.

Figure 7 | **Daily precipitation for Nairobi, as modeled by one of the models selected for low historical deviation from observed values (2050–2070)**

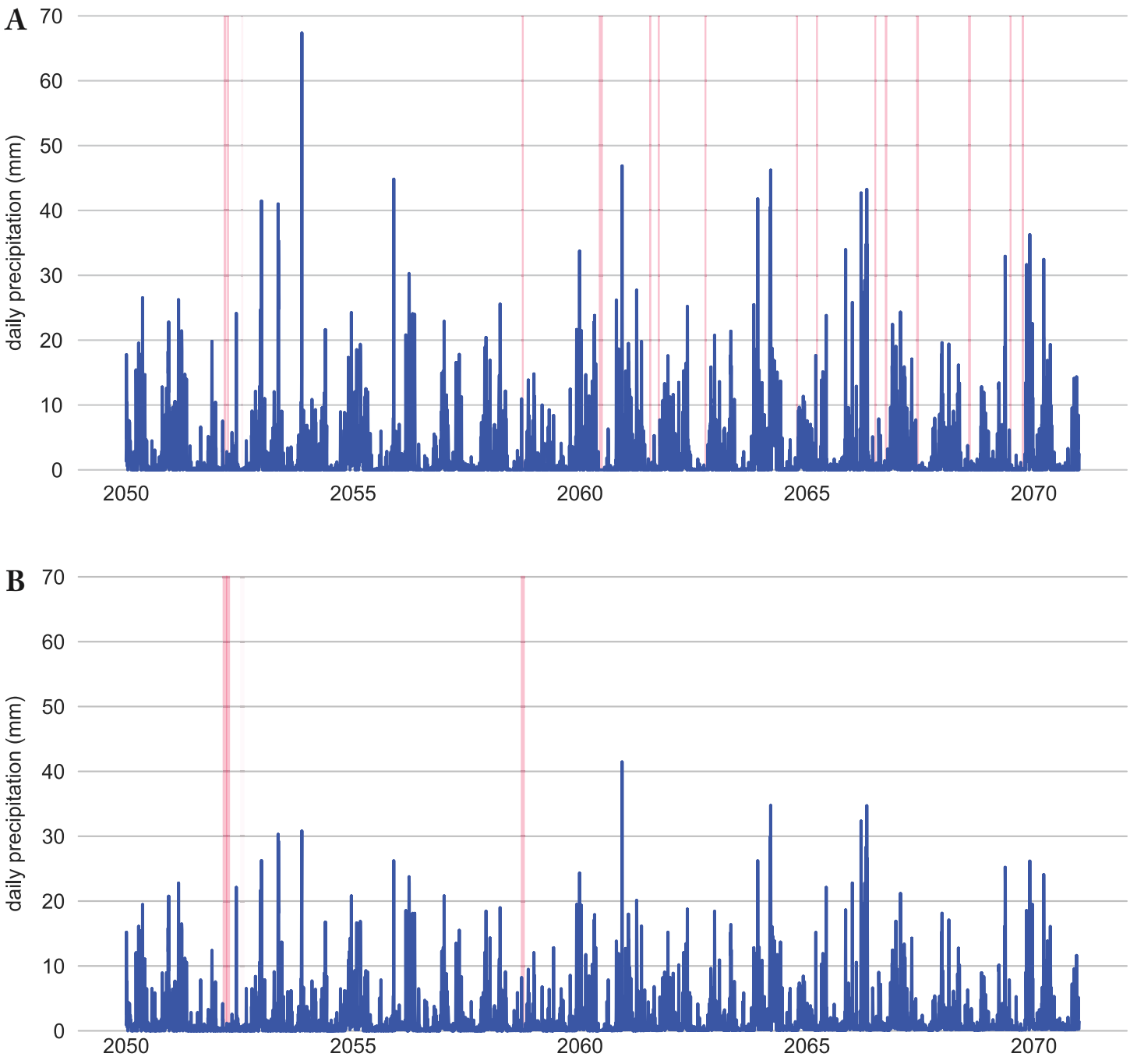

Figure 7 | **Daily precipitation for Nairobi, as modeled by one of the models selected for low historical deviation from observed values (2050–2070) (continued)**

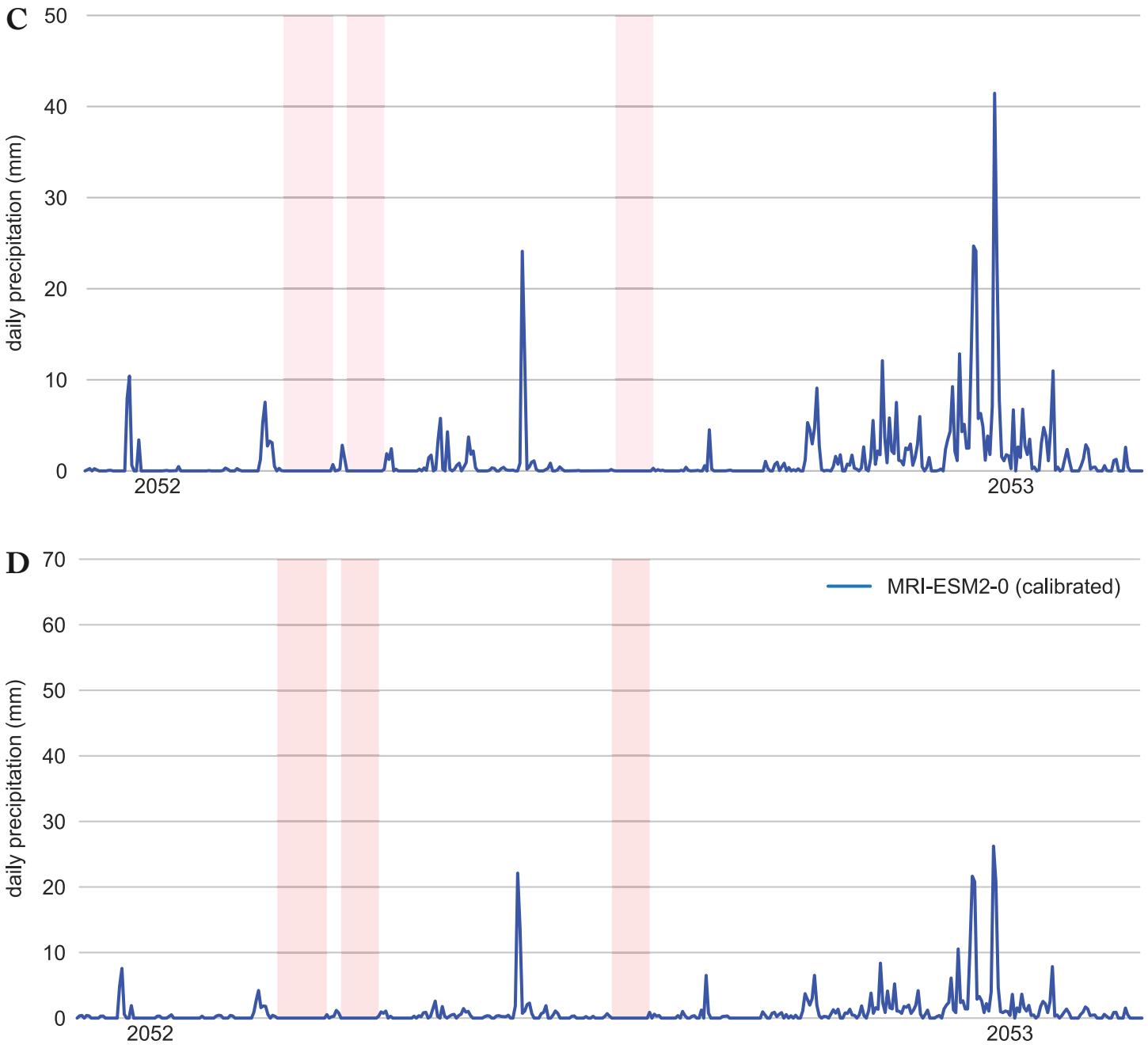

Notes: Dry spells (consecutive runs of days with zero precipitation) of at least 15 days are shaded pink. Panel A presents the uncalibrated time series. Panel B shows the calibrated time series and uses the seasonal calibration plots shown in Figure 6. Panel C (uncalibrated precipitation time series) and Panel D (calibrated precipitation time series) provide close-ups showing dry spells in 2052.

Source: WRI authors.

The total counts, *C*, of dry spell events during 2050–70 in Nairobi, as derived from the three best models, calibrated—MRI-ESM2-0, IPSL-CM6A-LR, and HadGEM3-GC31-MM—were, respectively, $C = 4, 5$, and 1. The count, *C*, is modeled probabilistically as the outcome of a Poisson random variable, with mean parameter *r* (see "Estimates of climate hazard frequencies and their uncertainty"). The resulting posterior distribution of the unknown Poisson parameter, *r*, is a unit-scaled gamma distribution with mean $C + {}^{1}/_{2}$.

The resulting predictive uncertainty distribution for the 21-year dry spell count is the gamma-Poisson distribution (see the method in "Estimates of climate hazard frequencies and their uncertainty"). This future period count uncertainty is represented by the histograms for the selected climate models: MRI-ESM2-0, IPSL-CM6A-LR, and HadGEM3-GC31-MM (Figure 8). They describe the estimated probabilities of various dry spell counts over the specified 21-year future period. The respective mean event counts are 4.5, 5.5, and 1.5. Although HadGEM3-GC31-MM has a notably different dry spell count prediction than the other models, it was selected based on its fit to observed data during the historical period 1980–2014.[2]

Figure 8 | **Predicted distributions for future Nairobi dry spell counts from the three downscaled climate models (2050-2070)**

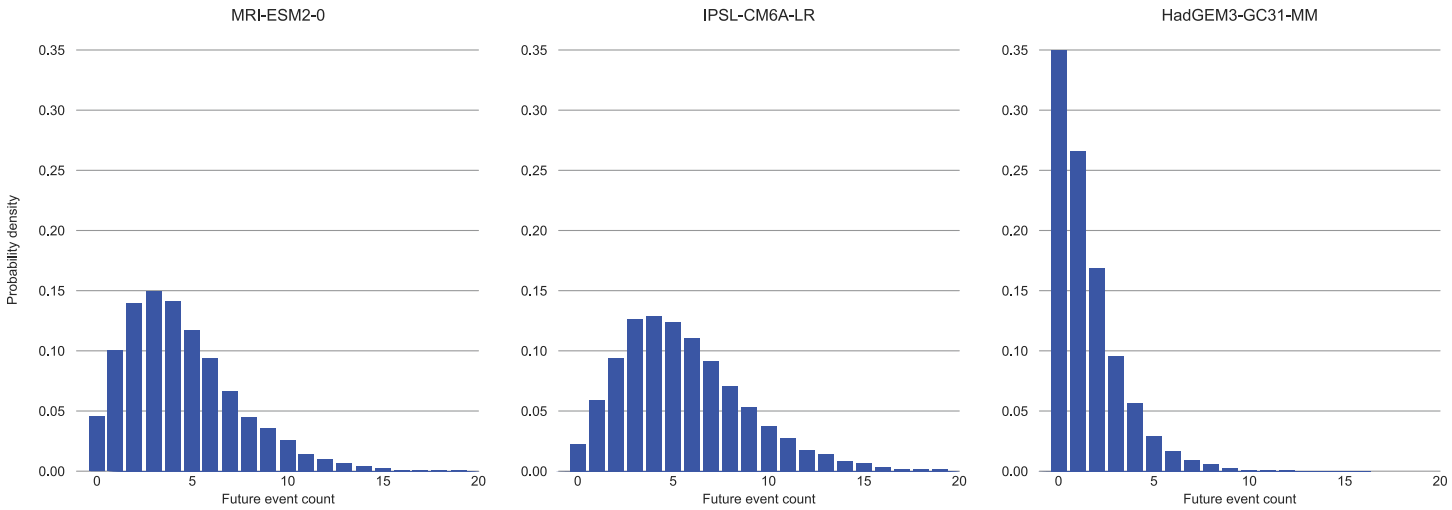

Notes: The mean predicted counts are 4.5, 5.5, and 1.5, respectively. HadGEM3-C31-MM has notably different dry spell count predictions than the other two selected climate models.
Source: WRI authors.

APPLICATIONS

These methods are versatile and can be applied to a wide variety of decision domains. Below, we outline some domains in which we have either applied or contemplated applying them.

Agriculture. Crops and their pests have physiological tolerance ranges that lend themselves well to hazard definition in our method. For example, Pezzopane et al. (2008) estimate that an economically important cultivar of *Coffea arabica* requires 2,887 degree-days above a 10.2°C base temperature between planting and harvest. We can define successful accumulation of these degree-days as a Bernoulli-modeled event and estimate the probability that this event occurs once per year. We intend to use this and related event definitions to support decision-making in the agricultural supply chain as part of WRI's AgriAdapt platform.

Energy planning. Degree-day calculations are frequently used in estimating capacity requirements and energy use in building heating and cooling systems. For example, the American Society of Heating, Refrigerating and Air-Conditioning Engineers publishes a set of standardized climate zones to be used in designing heating and cooling systems (ASHRAE 2021). The zones are defined in terms of degree-days and other climate indicators, all of which can be accommodated by our method.

Public health (heat waves). Researchers take numerous approaches to modeling heat and heat waves, many of which lend themselves well to our method. For example, Kim et al. (2023) find that deaths in Japan increase substantially when minimum nighttime temperatures stay at or above 25°C or the prefecture's 95th percentile of minimum temperature. We can estimate probabilities of future hot night occurrences using threshold temperatures like these and the calculations detailed above in "Summary of steps to estimate future climate hazard event occurrence frequencies."

Public health (infectious diseases). Some modes of disease transmission are at least partially mediated by climate-sensitive factors. For example, Mordecai et al. (2017) find that mosquito-borne arboviruses such as Zika, dengue, and chikungunya are most readily transmitted when the temperature is between 26°C and 29°C. We can use temperature ranges like this to estimate the number of future high-risk days for transmitting these diseases.

Disaster risk reduction (landslides). The landslide hazard indicator, as defined in Emberson et al. (2020), includes two conceptual elements: landslide susceptibility—which arises from natural topography and substrate material (it does not include effects of human-made impervious surfaces)—and the amount of heavy rainfall in the past six days. Practically, it requires calculating the antecedent rainfall index (ARI), comparing ARI to the historical 95th percentile of ARI, and overlaying the ARI comparison on the susceptibility map.

For the Data Portal for Cities adaptation pilot, we obtained an ARI 95th percentile map and landslide susceptibility map from NASA's Landslide Hazard Assessment for Situational Awareness (LHASA) project.[3] We then calculated future ARI-modeled precipitation time series and calculated a risk indicator as the number of days each year that a location with high susceptibility experiences ARI greater than its local 95th percentile.

Worker safety. More than 1 billion agricultural workers, road and construction crews, and other outdoor workers face health risks and even death from high-heat conditions (Ebi et al. 2021). Vecellio et al. (2022) find extended exposure to a wet-bulb globe temperature (T_w) of 30°C–31°C to be potentially lethal. Our method allows for estimation of future risk of worker illness and death or of constraints on agricultural and economic productivity.

We use the Stull (2011) formula for T_w:

$$T_w = T \cdot \arctan\left[0.151977(RH + 8.313659)^{\frac{1}{2}}\right] + \arctan(T + RH) - \arctan(RH - 1.676311) + 0.00391838 \cdot RH^{\frac{3}{2}} \cdot \arctan(0.023101RH) - 4.686035$$

where RH is relative humidity expressed as a percentage (e.g., "65" for "65 percent humidity"). For T, air temperature in degrees Celsius, we use maximum daily temperature. The ERA5 data set does not report RH, but it does report dewpoint temperature, D_p; thus, to calculate T_w for the observed data, first we calculate RH using this formula from Alduchov and Eskridge (1996):

$$RH = \frac{\exp\left(\frac{17.625D_p}{243.04 + D_p}\right)}{\exp\left(\frac{17.625T}{243.04 + T}\right)}$$

LIMITATIONS

These are some limitations of the hazard estimation methods:

Hazard indicator constraints. Our method for estimating counts of geographically localized future hazard events can only accommodate events whose occurrences are determined from the daily time series of four weather variables: minimum temperature, maximum temperature, daily precipitation, and daily average relative humidity.

Downscaled data limitations. Our downscaled climate models typically do not model land use and cannot distinguish urban land from rural land or wilderness. Our data may not, therefore, reflect factors not accounted for in the downscaling process, such as urban heat islands.

Climate model selection. Different climate models will typically provide different estimated future occurrence counts for a prescribed hazard event at a chosen location. For conciseness, we show hazard estimates derived from a best model from each of three model families. Thus, after recalibration, remaining uncorrected model biases are not incorporated into the uncertainties reflected in model-specific prediction histograms. Model biases are not random errors.

There is no clear basis for combining estimates from different selected models or to expect cancellation of model errors when model outputs are averaged. Therefore, predictions for the selected climate models are shown separately and compared.[4] When future hazard occurrence rate estimates from different models are similar, there is no real benefit in their combination; when they differ, it is best to exhibit the disagreement among climate model estimates.

Future greenhouse gas scenarios. We use climate model outputs derived from a particular future greenhouse gas emissions scenario. Different scenarios would yield different estimates for future hazard event occurrences.

Spatial resolution. We currently use models and historical observation data with spatial resolution of approximately 25–30 km. This resolution is not sufficiently fine for many urban and agricultural decision-making applications. Our method does not depend on the resolution of the input data, so it should be applicable to higher-resolution data if they become available.

Model calibration. Future hazard estimates are derived from recalibrated time series and are conditional on our historically derived calibration plots of observed versus model data for the historical period 1980–2014. Calibration is only an approximation of how future model data will differ from future observational data. Calibration uncertainty is not evaluated absent ensemble data from individual models. The calibrations are based on matching marginal distributions rather than matching day-to-day values.

Probabilistic modeling of prediction uncertainties. Inevitably, quantification of estimation uncertainty requires choosing a probability model as the data-generating mechanism (see "Estimates of climate hazard frequencies and their uncertainty"). Although the probability model used to characterize future hazard event uncertainty is adjusted to data, the appropriateness of the probability structure cannot be assured.

Climate model biases. The uncertainties reflected in the distribution of future event counts that we exhibit do not reflect climate model biases introduced by incorrect assumptions of future greenhouse gas emissions, or modeling errors resulting from incomplete specification of model dynamics. Even when climate models have shown small biases on larger geographic scales, they may still exhibit appreciable local biases. Our climate model selection and calibration are meant to reduce model bias for a historical period with available corresponding observations, but future biases may not be adequately corrected by methods based on past-data recalibration.

Timescale. Model timescales seldom match the timescale of modeled phenomena. As a result, climate models and our analyses can fail to capture some climate dynamics and changes to the parameters of our probability models. Sensitivity analysis might be useful for determining whether different time-step lengths are important in understanding specific climate hazards in particular locations.

ABBREVIATIONS

ARI	antecedent rainfall index
CMIP6	Coupled Model Intercomparison Project Phase 6 (CMIP6)
CSIRO	Commonwealth Scientific and Industrial Research Organisation
ESGF	Earth System Grid Federation
GCM	global climate model
GCoM	Global Covenant of Mayors for Climate and Energy
LHASA	Landslide Hazard Assessment for Situational Awareness
NASA	National Aeronautics and Space Administration
P-P	percentile-percentile
RMSE	root-mean-square error
SSP	Shared Socioeconomic Pathway

ENDNOTES

1. For more information about the ThinkHazard! tool, see https://thinkhazard.org/en/.
2. The Python code used for these examples is available in Jupyter notebooks at the GitHub repository, https://github.com/wri/cities-probabilistic-indicators/.
3. These data sets are available from the LHASA GitHub repository: https://github.com/nasa/LHASA.
4. See the discussion related to difficulties in combining predictions from climate models in Knutti et al. (2010) and the discussion on the question of model weighting in Wootten et al. (2023).

REFERENCES

Alduchov, O.A., and R.E. Eskridge. 1996. "Improved Magnus Form Approximation of Saturation Vapor Pressure." *Journal of Applied Meteorology and Climatology* 35 (4): 601–9. https://doi.org/10.1175/1520-0450(1996)035<0601:IMFAOS>2.0.CO;2.

Arnell, N.W. 2022. "The Implications of Climate Change for Emergency Planning." *International Journal of Disaster Risk Reduction* 83 (December): 103425. https://doi.org/10.1016/j.ijdrr.2022.103425.

ASHRAE (American Society of Heating, Refrigerating and Air-Conditioning Engineers). 2021. *Climatic Data for Building Design Standards*. Peachtree Corners, GA: ASHRAE. https://www.ashrae.org/file%20library/technical%20resources/standards%20and%20guidelines/standards%20addenda/169_2020_a_20211029.pdf.

Burillo, D., M.V. Chester, B. Ruddell, and N. Johnson. 2017. "Electricity Demand Planning Forecasts Should Consider Climate Non-stationarity to Maintain Reserve Margins during Heat Waves." *Applied Energy* 206 (November): 267–77. https://doi.org/10.1016/j.apenergy.2017.08.141.

Ebi, K.L., A. Capon, P. Berry, C. Broderick, R. de Dear, G. Havenith, Y. Honda, et al. 2021. "Hot Weather and Heat Extremes: Health Risks." *Lancet* 398 (10301): 698–708. https://doi.org/10.1016/S0140-6736(21)01208-3.

ECMWF (European Centre for Medium-Range Weather Forecasts). 2022. "ERA5: Data Documentation." July 14. https://confluence.ecmwf.int/display/CKB/ERA5%3A+data+documentation.

Emberson, R., D. Kirschbaum, and T. Stanley. 2020. "New Global Characterisation of Landslide Exposure." *Natural Hazards and Earth System Science* 20 (12): 3413–24. https://doi.org/10.5194/nhess-20-3413-2020.

Eyring, V., S. Bony, G.A. Meehl, C.A. Senior, B. Stevens, R.J. Stouffer, and K.E. Taylor. 2016. "Overview of the Coupled Model Intercomparison Project Phase 6 (CMIP6) Experimental Design and Organization." *Geoscientific Model Development* 9 (5): 1937–58. https://doi.org/10.5194/gmd-9-1937-2016.

GCoM (Global Covenant of Mayors for Climate and Energy). 2018. *Global Covenant of Mayors Common Reporting Framework*. Version 6.1. Brussels: GCoM Secretariat. https://www.globalcovenantofmayors.org/wp-content/uploads/2019/04/FINAL_Data-TWG_Reporting-Framework_website_FINAL-13-Sept-2018_for-translation.pdf.

GCoM. 2023. (Database.) *Data Portal for Cities*. https://dataportalforcities.org/. Accessed on 21 November 2023.

Holmgren, E.B. 1995. "The P-P Plot as a Method for Comparing Treatment Effects." *Journal of the American Statistical Association* 90 (429) 360–5. https://doi.org/10.1080/01621459.1995.10476520.

Iturbide, M., J. Fernández, J.M. Gutiérrez, J. Bedia, E. Cimadevilla, J. Díez-Sierra, R. Manzanas, et al. 2022. "Implementation of FAIR Principles in the IPCC: The WG1 AR6 Atlas Repository." *Scientific Data* 9 (629). https://doi.org/10.1038/s41597-022-01739-y.

Kim, S.E., M. Hashizume, B. Armstrong, A. Gasparrini, K. Oka, Y. Hijioka, A.M. Vicedo-Cabrera, and Y. Honda. 2023. "Mortality Risk of Hot Nights: A Nationwide Population-Based Retrospective Study in Japan." *Environmental Health Perspectives* 131 (5): 057005. https://doi.org/10.1289/EHP11444.

Knutti, R., R. Furrer, C. Tebaldi, J. Cermak, and G.A. Meehl. 2010. "Challenges in Combining Projections from Multiple Climate Models." *Journal of Climate* 23 (10): 2739–58. https://doi.org/10.1175/2009JCLI3361.1.

Kuma, P., F.A.-M. Bender, and A.R. Jönsson. 2023. "Climate Model Code Genealogy and Its Relation to Climate Feedbacks and Sensitivity." *Journal of Advances in Modeling Earth Systems* 15 (7): e2022MS003588. https://doi.org/10.1029/2022MS003588.

Moda, H.M., W.L. Filho, and A. Minhas. 2019. "Impacts of Climate Change on Outdoor Workers and Their Safety: Some Research Priorities." *International Journal of Environmental Research and Public Health* 16 (18): 3458. https://doi.org/10.3390/ijerph16183458.

Mordecai, E.A., J.M. Cohen, M.V. Evans, P. Gudapati, L.R. Johnson, C.A. Lippi, K. Miazgowicz, et al. 2017. "Detecting the Impact of Temperature on Transmission of Zika, Dengue, and Chikungunya Using Mechanistic Models." *PLoS Neglected Tropical Diseases* 11 (4): e0005568. https://doi.org/10.1371/journal.pntd.0005568.

NASA (National Aeronautics and Space Administration). 2023. "NASA Earth Exchange Global Daily Downscaled Projections (NEX-GDDP-CMIP6)." August 27. https://www.nccs.nasa.gov/sites/default/files/NEX-GDDP-CMIP6-Tech_Note.pdf.

Nasr, A., I. Björnsson, D. Honfi, O.L. Ivanov, J. Johansson, and E. Kjellström. 2021. "A Review of the Potential Impacts of Climate Change on the Safety and Performance of Bridges." *Sustainable and Resilient Infrastructure* 6 (3–4): 192–212. https://doi.org/10.1080/23789689.2019.1593003.

Ngonghala, C.N., S.J. Ryan, B. Tesla, L.R. Demakovsky, E.A. Mordecai, C.C. Murdock, and M.H. Bonds. 2021. "Effects of Changes in Temperature on Zika Dynamics and Control." *Journal of the Royal Society Interface* 18 (178): 20210165. https://doi.org/10.1098/rsif.2021.0165.

Pezzopane, J.R.M., M.J.P. Júnior, M.B.P. de Camargo, and L.C. Fazuoli. 2008. "Exigência térmica do café arábica cv. Mundo Novo no subperíodo florescimento-colheita." *Ciência e Agrotecnologia* 32 (6): 1781–86. https://doi.org/10.1590/S1413-70542008000600016.

Riahi, K., D.P. van Vuuren, E. Kriegler, J. Edmonds, B.C. O'Neill, S. Fujimori, N. Bauer, et al. 2017. "The Shared Socioeconomic Pathways and Their Energy, Land Use, and Greenhouse Gas Emissions Implications: An Overview." *Global Environmental Change* 42: 153–68. https://doi.org/10.1016/j.gloenvcha.2016.05.009.

Rocklöv, J., and Y. Tozan. 2019. "Climate Change and the Rising Infectiousness of Dengue." *Emerging Topics in Life Sciences* 3 (2): 133–42. https://doi.org/10.1042/ETLS20180123.

Sanderson, B.M., M. Wehner, and R. Knutti. 2017. "Skill and Independence Weighting for Multi-model Assessment." *Geoscientific Model Development* 10 (6): 2379–95. https://doi.org/10.5194/gmd-10-2379-2017.

Schwalm, C.R., S. Glendon, and P.B. Duffy. 2020. "RCP8.5 Tracks Cumulative CO_2 Emissions." *Proceedings of the National Academy of Sciences of the United States of America* 117 (33): 19656–57. https://doi.org/10.1073/pnas.2007117117.

Stull, R. 2011. "Wet Bulb Temperature from Relative Humidity and Air Temperature." *Journal of Applied Meteorology and Climatology* 50 (11): 2267–69. https://doi.org/10.1175/JAMC-D-11-0143.1.

Thornton, P.K., P.J. Ericksen, M. Herrero, and A.J. Challinor. 2014. "Climate Variability and Vulnerability to Climate Change: A Review." *Global Change Biology* 20 (11): 3313–28. https://doi.org/10.1111/gcb.12581.

Vecellio, D.J., S.T. Wolf, R.M. Cottle, and W.L Kenney. 2022. "Evaluating the 35°C Wet-Bulb Temperature Adaptability Threshold for Young, Healthy Subjects (PSU HEAT Project)." *Journal of Applied Physiology* 132 (2): 340–45. https://doi.org/10.1152/japplphysiol.00738.2021.

Wang, W., S. Yang, H.E. Stanley, and J. Gao. 2019. "Local Floods Induce Large-Scale Abrupt Failures of Road Networks." *Nature Communications* 10 (May): 2114. https://doi.org/10.1038/s41467-019-10063-w.

Wootten, A.M., E.C. Massoud, D.E. Waliser, and H. Lee. 2023. "Assessing Sensitivities of Climate Model Weighting to Multiple Methods, Variables, and Domains in the South-Central United States." *Earth System Dynamics* 14 (1): 121–45. https://doi.org/10.5194/esd-14-121-2023.

World Bank. n.d. (Database.) *Climate Change Knowledge Portal*. https://climateknowledgeportal.worldbank.org/. Accessed November 20, 2022.

ACKNOWLEDGMENTS

We are pleased to acknowledge our institutional strategic partners that provide core funding to WRI: the Netherlands Ministry of Foreign Affairs, Royal Danish Ministry of Foreign Affairs, and Swedish International Development Cooperation Agency.

We also acknowledge the Global Covenant of Mayors for Climate and Energy, the Walmart Foundation, and Bloomberg Philanthropies.

ABOUT THE AUTHORS

Theodore Wong is a Research and Project Associate at WRI Ross Center for Sustainable Cities.
Contact: ted.wong@wri.org

Paul Switzer is Stanford University Professor Emeritus of Statistics and Earth System Science.
Contact: switzer@stanford.edu

ABOUT WRI

World Resources Institute is a global research organization that turns big ideas into action at the nexus of environment, economic opportunity, and human well-being.

Our challenge

Natural resources are at the foundation of economic opportunity and human well-being. But today, we are depleting Earth's resources at rates that are not sustainable, endangering economies and people's lives. People depend on clean water, fertile land, healthy forests, and a stable climate. Livable cities and clean energy are essential for a sustainable planet. We must address these urgent, global challenges this decade.

Our vision

We envision an equitable and prosperous planet driven by the wise management of natural resources. We aspire to create a world where the actions of government, business, and communities combine to eliminate poverty and sustain the natural environment for all people.

Our approach

COUNT IT

We start with data. We conduct independent research and draw on the latest technology to develop new insights and recommendations. Our rigorous analysis identifies risks, unveils opportunities, and informs smart strategies. We focus our efforts on influential and emerging economies where the future of sustainability will be determined.

CHANGE IT

We use our research to influence government policies, business strategies, and civil society action. We test projects with communities, companies, and government agencies to build a strong evidence base. Then, we work with partners to deliver change on the ground that alleviates poverty and strengthens society. We hold ourselves accountable to ensure our outcomes will be bold and enduring.

SCALE IT

We don't think small. Once tested, we work with partners to adopt and expand our efforts regionally and globally. We engage with decision-makers to carry out our ideas and elevate our impact. We measure success through government and business actions that improve people's lives and sustain a healthy environment.